Battery Health Prognosis for Electric Vehicles Using Sample Entropy and Sparse Bayesian Predictive Modeling

Xiaosong Hu, *Member, IEEE*, Jiuchun Jiang, *Senior Member, IEEE*, Dongpu Cao, *Member, IEEE*, and Bo Egardt, *Fellow, IEEE*

***Abstract*—Battery health monitoring and management is of extreme importance for the performance and cost of electric vehicles. This paper is concerned with machine-learning-enabled battery state-of-health (SOH) indication and prognosis. The sample entropy of short voltage sequence is used as an effective signature of capacity loss. Advanced sparse Bayesian predictive modeling (SBPM) methodology is employed to capture the underlying correspondence between the capacity loss and sample entropy. The SBPM-based SOH monitor is compared with a polynomial model developed in our prior work. The proposed approach allows for an analytical integration of temperature effects such that an explicitly temperature-perspective SOH estimator is established, whose performance and complexity is contrasted to the support vector machine (SVM) scheme. The forecast of remaining useful life is also performed via a combination of SBPM and bootstrap sampling concepts. Large amounts of experimental data from multiple lithium-ion battery cells at three different temperatures are deployed for model construction, verification, and comparison. Such a multi-cell setting is more useful and valuable than only considering a single cell (a common scenario). This is the first known application of combined sample entropy and SBPM to battery health prognosis.**

***Index Terms*—Bayesian inference, electric vehicle, energy storage, health monitoring, lithium-ion battery, machine learning.**

I. Introduction

A. Motivation and Technical Challenge

ENERGY storage has been recognized as a crucial enabling technology for improving energy sustainability in both the transportation and electricity sectors [1]–[4]. Batteries are widely utilized in portable electronic devices, electric vehicles, and power grids. With increasing vehicle-to-grid synergies and renewable energy integration, batteries are uniquely positioned to play an imperative role [5]–[7]. In spite of considerable progress in battery chemistry and material, battery systems are still usually oversized and underused, i.e., 20%–50% excess energy capacity is provided, which evokes augmented weight, volume, and purchase cost [8]. Attenuation of this conservatism necessitates an efficient battery management system, in which critical internal variables, e.g., state-of-charge (SOC), state-of-power, and state-of-health (SOH), are accurately monitored [9]–[13]. Particularly, appropriate battery health management facilitates avoiding catastrophic hazards and premature failure, and thus improving battery durability.

The battery SOH is generally applied to evaluate the degree of battery degradation. Its characterization, assessment, and prognosis, however, is particularly challenging in electric vehicle applications, since: 1) various degradation processes with distinct spatiotemporal dynamics arise, such as material stress and fatigue, electrode delamination, electrolyte decomposition, solid electrolyte interface (SEI) growth, and lithium deposition in lithium-ion batteries [14]; 2) the path dependence of certain degradation phenomena is intricate; and 3) the operating regime is volatile in terms of load and temperature profiles. Meanwhile, these challenges constitute a major incentive to take advantage of advanced diagnosis and prognosis methodologies [15]–[17]. In this paper, we aim to devise a data-driven SOH forecasting model based upon a combination of sample entropy and Bayesian inference, because data-driven control, monitoring, and fault diagnosis and isolation [18], [19] is a thriving area of research in both academia and industry.

B. Literature Review

Research on the battery SOH monitoring and prediction is rather intensive, and a plethora of relevant estimation models/techniques have been reported. Several review papers have been published to summarize state-of-the-art SOH estimation methods, concluding that each has its own strengths and limitations [20], [21]. These methods can be principally classified into three categories: 1) direct measurement; 2) model-based approach; and 3) data-driven approach.

1) Direct Measurement: Direct measurement means that completely full charging and discharging processes are used

Manuscript received January 19, 2015; revised March 25, 2015 and April 30, 2015; accepted June 6, 2015. Date of publication July 28, 2015; date of current version March 8, 2016. The work of D. Cao was supported by the UK EPSRC "FUTURE Vehicles" project under Grant EP/I038586/1. *(Corresponding authors: Xiaosong Hu and Jiuchun Jiang.)*

X. Hu is with the National Active Distribution Network Technology Research Center, Beijing Jiaotong University, Beijing 100044, China, and also with the Department of Civil and Environmental Engineering, University of California, Berkeley, CA 94720 USA (e-mail: xiaosonghu@ieee.org).

J. Jiang is with the National Active Distribution Network Technology Research Center, Beijing Jiaotong University, Beijing 100044, China (e-mail: jcjiang@bjtu.edu.cn).

D. Cao is with the Center for Automotive Engineering, Cranfield University, Bedford, MK43 0AL, U.K. (e-mail: d.cao@cranfield.ac.uk).

B. Egardt is with the Department of Signals and Systems, Chalmers University of Technology, 41296 Gothenburg, Sweden (e-mail: bo.egardt@chalmers.se).

Color versions of one or more of the figures in this paper are available online at http://ieeexplore.ieee.org.

Digital Object Identifier 10.1109/TIE.2015.2461523

to calibrate the battery static capacity. For example, constant-current and constant-voltage charge/discharge procedure is often recommended for lithium-ion batteries. In [22], direct capacity measurement is incorporated into an enhanced Coulomb counting-based SOC meter. This scheme is straightforward, but has only limited application, e.g., specialized laboratory environment. Electric vehicles are never fully charged or discharged in realistic operations. Additionally, it is time consuming and impairs the battery lifespan to a certain extent.

2) Model-Based Approach: Main model-based approaches reported in the literature can be further divided into two subgroups: 1) degradation modeling; and 2) state/parameter observer. For characterizing battery aging mechanisms, diverse electrochemical models emerged. For instance, an electrochemical model has been established in [23] and [24] to mimic the SEI growth of a lithium-ion cell and to describe its impact on the cell capacity loss. A single-particle model with several refined parameters was also derived to probe capacity-decay sources of a graphite/LiFePO4 cell in both storage and cycling conditions [25]. The model indicated that the cell capacity fade during storage was merely caused by the loss of cyclable lithium, whereas that during cycling was induced by additional loss of graphite active material. These models enable a fundamental understanding of spatiotemporal dynamics of electrochemical reactions inside batteries and give theoretical/physical interpretations of some battery aging symptoms. Nonetheless, these electrochemistry-based aging models did not directly resolve SOH prediction issues. Moreover, they are still not well-prepared for pragmatic use because of complicated partial differential equations. Some relatively simple semi-empirical performance models were built to represent the dependence of battery SOH on likely stressing factors. For example, an Arrhenius-like model has been created to portray the capacity fade of graphite/LiFePO4 cells as a function of depth-of-discharge (DOD), temperature, and C-rate [26]. A mechanical fatigue model based on Palmgren–Miner (PM) principle was also formulated to emulate damage accumulation of lithium-ion batteries for lifetime prediction [27]. While these simpler models provide no insights into detailed electrochemical processes incurring battery degradation, they can be conveniently leveraged to reveal the influence of stressing factors on the battery SOH. Of course, the performance of these semi-empirical models highly depends on the quality and quantity of testing data.

Another model-based methodology is focused on state/parameter observer design, as the battery SOH monitoring problem can be mathematically cast as a parameter estimation problem. A broad variety of SOH observers were proposed, where reduced-order electrochemical and electrical-circuit models were adopted. Key scenarios comprise dual/joint extended Kalman filtering (EKF) [28], dual sliding-mode observer [29], particle filter [30], etc. These observer-based techniques are online and closed-loop. Their effectiveness and adaptability are, however, sensitive to the credibility and robustness of the prescribed battery models.

3) Data-Driven Approach: Data-driven approaches are gaining increasing attention in both academia and industry, as a result of their flexibility and model-free characteristics. This type of method can be grouped into four principle subclasses: 1) directly mapping from aging cycle to SOH; 2) mapping from achievable variables (stressing factors or features extracted) to SOH; 3) signal processing; and 4) statistical metrics. For instance, Rezvani *et al.* compared two black-box modeling procedures (i.e., adaptive neural network and linear prediction error method) for lithium-ion battery SOH estimation by directly using the capacity-cycle data pairs [31]. The Dempster–Shafer theory and Bayesian Monte Carlo methodology were also employed to capture the underlying generative mechanism of the capacity-cycle data pairs [32]. The battery aging cycles need to be precisely known for this subclass of model, which turns out to be impractical, particularly for hybrid electric vehicles. Instead, in the second subclass of method, some readily measurable variables (e.g., historical SOC, temperature, and current) or representative features extracted act as the inputs of black-box models, such as artificial neural networks [33], [34], fuzzy logic [35], and support vector machine (SVM) [36]. Signal processing was also used for *in situ* diagnosis of battery degradation, including incremental capacity analysis (ICA) [37], differential voltage analysis (DVA) [38], differential thermal voltammetry (DTV) [39], and so forth. To produce battery SOH estimates, this class of differential signal requires further manipulation via classification and/or regression techniques, e.g., SVM in [40].

In addition, a spectrum of statistical metrics was put forward for battery health assessment. For example, statistical dependence exploration was conducted to examine the major factors effecting performance deterioration of a lithium-ion battery in real-world electric vehicle use [41]. A sample entropy-based capacity estimator for a lithium-ion battery was synthesized in [42]. As a signature symptomatic of capacity fade, the sample entropy of voltage observations collected in a complete constant-current discharge process was picked as the estimator input. Unfortunately, such a treatment is very costly and even unfeasible in electric vehicles, owing to the long-time full discharge. In our prior work [43], based on merely short-term hybrid pulses, an enhanced sample entropy-based SOH monitoring scenario was designed, leading to greater convenience, applicability, and robustness.

The upsides and downsides of all the foregoing methods are summarized in Table I for a straightforward comparison.

C. Key Contributions

As an extension of [43], the primary objective of this paper is to explore the improvement potential of the sample entropy-based SOH gauge through advanced machine-learning tools. In contrast to a third-degree polynomial model in [43], sparse Bayesian predictive modeling (SBPM) approach is herein applied to extrapolate the correspondence between the capacity loss and sample entropy with the aim to upgrade the accuracy and robustness of SOH monitoring. There are four original important contributions. First, the Bayesian scheme in a univariate form is compared with the prior polynomial model at three different temperatures. Second, a multivariate Bayesian SOH estimation model is developed to analytically integrate temperature effects, and a comparison with the SVM scheme is made. Third, the prediction of remaining useful life (RUL) for lithium-ion batteries is performed via a synergy of SBPM and

TABLE I
SUMMARY OF ALL THE THREE CATEGORIES OF BATTERY SOH MONITORING METHODS: UPSIDES AND DOWNSIDES

Category	Subclass	Example	Upside	Downside
Direct measurement	-	[22]	Simple and straightforward	Poor applicability in electric vehicles; time-consuming; harmful to battery durability
Model-based methodology	1) Degradation modeling	Electrochemical models [23-25]	Theoretical/physical interpretations of some battery aging phenomena	Incapable of directly solving SOH estimation issues; heavy complexity
		Semi-empirical performance model [26], [27]	Moderate complexity; disclosure of the influences of stressing factors on SOH	No physical interpretations of aging sources; sensitive to the quantity and quality of battery data
	2) State/parameter observer	Dual/joint EKF [28], dual sliding mode observer [29], and particle filter [30]	Online and closed-loop	Relatively heavy computational burden; sensitive to precision and robustness of battery model
Data-driven methodology	1) Directly mapping from aging cycle to SOH	[31], [32]	Straightforward; good nonlinear mapping	Difficult implementation; sensitive to the quantity and quality of battery data
	2) Mapping from stressing factors or features extracted to SOH	Artificial neural networks [33], [34], fuzzy logic [35], and support vector machine (SVM) [36]	Relatively easy implementation; good nonlinear mapping; disclosure of the influences of related factors/ features to SOH	Sensitive to the quantity and quality of battery data
	3) Signal processing	ICA [37]; DVA [38]; DTV [39]	Simple; on-board diagnosis	Further manipulation needed to infer numerical SOH estimates
	4) Statistical metrics	Statistical dependency analysis [41]; sample entropy [42]; enhanced sample entropy [43]	Simple and straightforward, on-board applicability for enhanced sample entropy	Sensitive to the quantity and quality of battery data

bootstrap sampling concepts. Finally, it is worth underscoring that validation and comparison of all the models are executed in a multi-cell setting, which is more practical and meaningful than using the data of barely a single cell. This is the first known application of combined sample entropy and SBPM to battery health prognosis problems. Its stability issue in online vehicular environments is unaddressed herein, which is, however, anticipated in our future work, as an important aspect of complicated system performance monitoring in industrial practice [44].

D. Paper Organization

The rest of this article is outlined as follows. Section II presents a brief overview of the experimentation degrading lithium-ion batteries. The sample entropy and SBPM algorithms are introduced in Section III. Section IV discusses the verification and comparison outcomes. Conclusions are finally summarized in Section V.

II. Battery Testing and Degradation Data

Eight lithium nickel-manganese-cobalt oxide (LiNMC) UR14650P cells were placed in cell holders (the top layer) in a thermal chamber and independently tested in eight channels (Channels 17–24) of a battery cycler (see Fig. 1). The eight cells were loaded and degraded by the test procedure displayed in Fig. 2. Each experimental period is composed of three

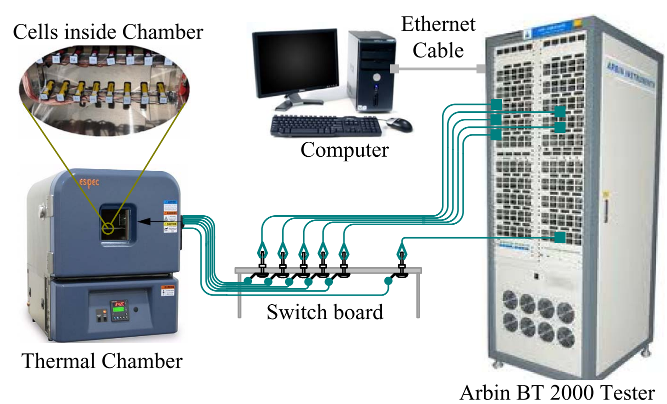

Fig. 1. Architecture of battery test bench [45]. The main specification of LiNMC cells is as follows: the nominal capacity and voltage are 0.94 Ah and 3.70 V, respectively; the upper and lower cutoff voltages are 4.20 and 2.50 V, respectively.

characterization tests at 10 °C, 22 °C, and 35 °C, the impedance test at 22 °C, and the degradation test (aging cycles) at 22 °C. About two weeks were taken to complete each period. More experimental details are referred to [45]. The degradation data that we consider here are measured capacities in the static capacity tests and voltage sequences under the HPPC (Hybrid Pulse Power Characterization) profiles in the hybrid pulse tests at the three different temperatures. For instance, the evolution of capacity over the degradation process at 10 °C is presented

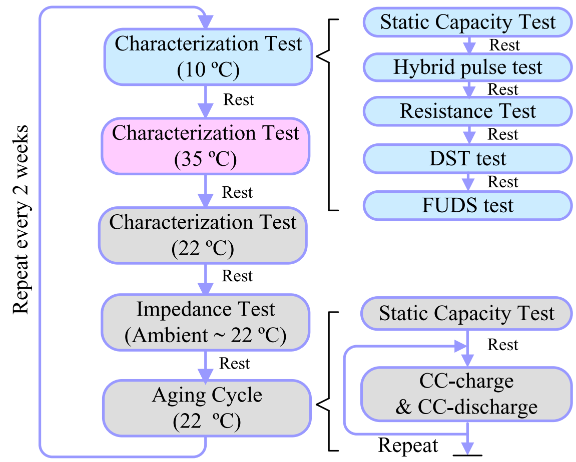

Fig. 2. Test procedure [45]. The hybrid pulse test is a sequence of pulse cycles with each being a concatenation of the standard HPPC profile and a self-designed discharging/charging pulse profile. The resistance test uses the standard testing program from Arbin to calibrate the internal resistance. The DST and FUDS are Dynamic Stress Test and Federal Urban Dynamic Scheduling Test, respectively. All the data constitutes a versatile database for research on various aspects of battery control and monitoring, such as peak-power estimation in [13], equivalent circuit modeling in [45], and health management [43]. The battery aging data at different temperatures are used in this paper.

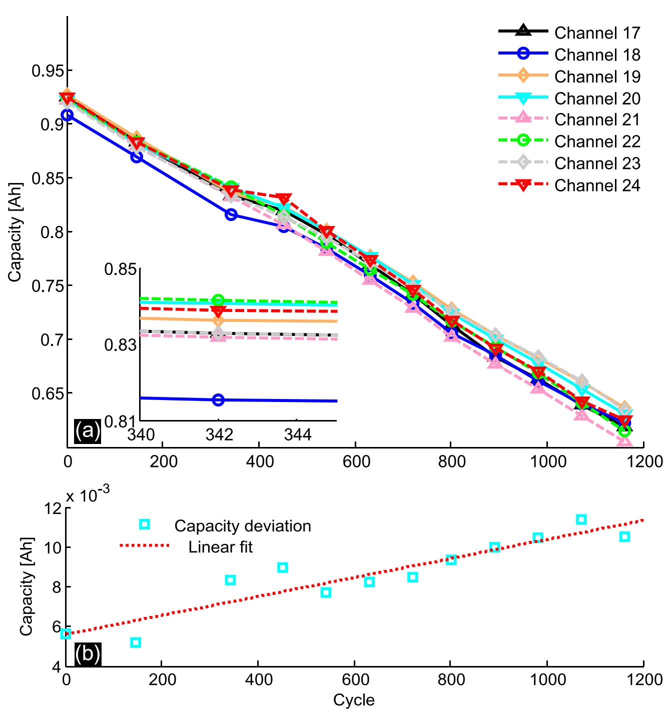

Fig. 3. Capacity evolution during battery aging at 10 °C: (a) capacity trajectory and (b) capacity deviation (the standard deviation of the capacities of the eight cells).

in Fig. 3. Capacity variance is visible among the eight cells. Such variance degree is slight, when the cells are fresh, and then becomes increasingly large with aging. The overall capacity deviation is, nevertheless, very small in well-governed testing conditions. Analogous outcomes are procured at 22 °C and 35 °C. Cell-to-cell or pack-to-pack imbalance also appears in realistic large-scale battery applications. Continually improved

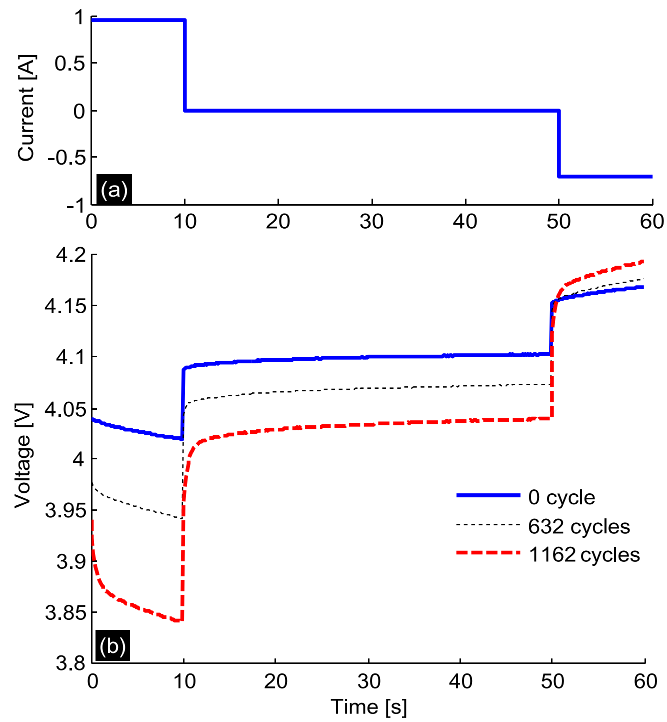

Fig. 4. Current and voltage behavior of the LiNMC cell (Channel 17, at around 90% SOC and 22 °C) under the HPPC profile with respect to different aging levels: (a) Current excitation, and (b) voltage response.

battery chemistry, manufacturing skills, and balancing systems are anticipated to alleviate such imbalance to a minute extent [46], [47]. As such, battery health forecaster trained using the data of reference cells could be trustworthy for other cells of the same chemistry and from the same batch. This motivates us to develop a multi-cell health prognosis paradigm that is more practically significant than the conventional single-cell scheme. Here, cells placed in Channels 17, 19, and 21 are randomly selected as reference cells, while the remainder serves as validation cells. The current and voltage behavior of the LiNMC cell (Channel 17, at about 90% SOC and 22 °C) under the HPPC excitation is displayed in Fig. 4. It is abundantly clear that the voltage response is highly sensitive to the cell health. More specifically, the degree of voltage fluctuation increases with cell aging, including both the static (instantaneous) and dynamic (relaxed) voltage transitions. The augment of static voltage change is explained by dc-resistance increase well, and the alteration in the imaginary part of the cell impedance largely induces enlarged dynamic voltage change. Therefore, the HPPC voltage sequence (involving charge, discharge, and rest) offers rich information to capture decaying battery health.

III. Machine-Learning-Oriented SOH Prognosis

A. Sample Entropy Algorithm

Sample entropy is a useful statistic for quantitatively assessing the fluctuation degree of a time series of length N_c. Hence, the sample entropy of the voltage sequence under the HPPC excitation could be an effective signature correlating to battery

TABLE II
SAMPLE ENTROPY ALGORITHM

Step 1: Assign the tunable parameters m and r. For a time series of length N_c, $\{s(k):1\le k_s\le N_c\}$, form the N_c-m+1 vectors $U_m(k_s)=\{s(k_s+l):0\le l\le m-1\},k_s=1,\dots,N_c-m+1$.
Step 2: The distance between two such vectors is defined as the maximum absolute difference of their scalar elements: $d\left[U_m(k_s),U_m(n)\right]=\max\{\lvert s(k_s+l)-s(n+l)\rvert:0\le l\le m-1\}$.
Step 3: The first N_c-m vectors of length m are considered such that for $k_s=1,\dots,N_c-m$, both $U_m(k_s)$ and $U_{m+1}(k_s)$ can be defined in the time series of length N_c.
Step 4: Define $B_{k_s}^m(r)=\frac{1}{N_c-m-1}W^m(k_s),k_s=1,\dots,N_c-m$ $A_{k_s}^m(r)=\frac{1}{N_c-m-1}W^{m+1}(k_s),k_s=1,\dots,N_c-m$ where $W^m(k_s)$ is the number of vectors $U_m(n)$ that make $d\left[U_m(k_s),U_m(n)\right]\le r$ for $n=1,\dots,N_c-m$ $(n\ne k_s)$. Similarly, $W^{m+1}(k_s)$ is the number of vectors $U_{m+1}(n)$ that make $d\left[U_{m+1}(k_s),U_{m+1}(n)\right]\le r$ for $n=1,\dots,N_c-m$ $(n\ne k_s)$.
Step 5: Define $B^m(r)=\frac{1}{N_c-m}\sum_{k_s=1}^{N_c-m}B_{k_s}^m(r)$, $A^m(r)=\frac{1}{N_c-m}\sum_{k_s=1}^{N_c-m}A_{k_s}^m(r)$, where $B^m(r)$ and $A^m(r)$ are probabilities that two sequences match for m and m+1 points, respectively.
Step 6: The sample entropy is ultimately estimated by $\mathrm{SampEn}(m,r,N_c)=-\ln\left[\frac{A^m(r)}{B^m(r)}\right]$.

health. The sample entropy SampEn(m, r, N_c) is defined to be the negative natural logarithm of an estimate of the conditional probability that windows of length m (subseries of the time series of length N_c) that remain similar within a tolerance r also match at the next point [48]. Self-matches are excluded during computing the conditional probability. The steps of sample entropy algorithm are detailed in Table II.

B. SBPM Algorithm

As an advanced machine-learning approach, the SBPM is utilized in this work to portray the correspondence between the voltage-sequence sample entropy and the battery capacity. Its basic principles are elucidated in the successive subsections.

1) Likelihood of All the Data Samples: The model input variables are denoted by $\boldsymbol{x}_i$, $i=1,\dots,N_s$, where N_s is the number of data samples. For each $\boldsymbol{x}_i$, there is a corresponding real-valued target t_i, $i=1,\dots,N_s$, and the goal of SBPM is to learn the underlying functional mapping, based on such input–target pairs. In the SBPM framework, a generalized linear-in-parameter model is often considered, as described by

$$\hat{y}(\boldsymbol{x},\boldsymbol{w})=\sum_{j=1}^{M}w_j\varphi_j(\boldsymbol{x}) \tag{1}$$

where $\boldsymbol{w}=[w_1,\dots,w_M]^T$ is the vector of model parameters to be identified, φ is the basis function, M is the number of basis functions, and $\hat{y}$ is the estimated model output. Assume that the target data is a noisy implementation of (1), say $t_i=\hat{y}(\boldsymbol{x}_i,\boldsymbol{w})+\varepsilon_i$. Here, a Gaussian distribution over ε_i with mean zero and variance σ^2 is chosen, i.e., $p(\varepsilon_i|\sigma^2)=N(0,\sigma^2)$, and $p(t_i|\boldsymbol{w},\sigma^2)=N(\hat{y}(\boldsymbol{x}_i,\boldsymbol{w}),\sigma^2)$. Throughout this paper, p and N represent probability and normal distribution, respectively. Assuming that each sample is generated independently, the likelihood of all the data samples can be achieved by

$$p(\boldsymbol{t}|\boldsymbol{w},\sigma^2)=(2\pi\sigma^2)^{-N_s/2}\exp\left(-\frac{1}{2\sigma^2}\|\boldsymbol{t}-\boldsymbol{\Phi}\boldsymbol{w}\|^2\right) \tag{2}$$

where $\boldsymbol{t}=[t_1,\dots,t_{N_s}]^T$ and $\boldsymbol{\Phi}$ is the $N_s\times M$ design matrix with $\boldsymbol{\Phi}_{ij}=\varphi_j(\boldsymbol{x}_i)$.

2) Sparse Bayesian Prior: Model sparsity is an intriguing notion, as it furnishes not only elegant complexity control and elucidation of relevant input variables but also practical advantages of computational speed, compactness, and tractability. To procure sparsity, the following Gaussian prior with mean zero is prescribed

$$p(\boldsymbol{w}|\gamma_1,\dots,\gamma_M)=\prod_{j=1}^{M}\left[(2\pi)^{-1/2}\gamma_j^{1/2}\exp\left(-\frac{1}{2}\gamma_j w_j^2\right)\right] \tag{3}$$

where M hyperparameters $\boldsymbol{\gamma}=[\gamma_1,\dots,\gamma_M]^T$ are used to regulate the inverse variances of M parameters $\boldsymbol{w}$, and (3) manifests the degree of belief over $\boldsymbol{w}$, i.e., a preference to simpler and smoother models by attaching larger prior probabilities to smaller parameters. The strength of such belief is moderated by $\boldsymbol{\gamma}$. It is clear that $\boldsymbol{w}$ tends to zero as $\boldsymbol{\gamma}$ becomes increasingly large, resulting in the model sparsity.

3) Parameter Posterior: Given the likelihood (2) and prior (3), the posterior distribution over parameters is derived by Bayes' rule

$$p(\boldsymbol{w}|\boldsymbol{t},\boldsymbol{\gamma},\sigma^2)=\frac{p(\boldsymbol{t}|\boldsymbol{w},\sigma^2)p(\boldsymbol{w}|\boldsymbol{\gamma})}{p(\boldsymbol{t}|\boldsymbol{\gamma},\sigma^2)}=N\left(\boldsymbol{\mu},\sum\right) \tag{4}$$

with

$$\begin{cases}\sum=(\sigma^{-2}\boldsymbol{\Phi}^T\boldsymbol{\Phi}+\boldsymbol{B})^{-1}\\ \boldsymbol{\mu}=\sigma^{-2}\sum\boldsymbol{\Phi}^T\boldsymbol{t}\end{cases} \tag{5}$$

where $\boldsymbol{B}$ is a diagonal matrix with $\boldsymbol{\gamma}$ being the main diagonal elements.

4) Maximum Marginal Likelihood Approximation: Treating $\boldsymbol{\gamma}$ and σ^2 as random variables and employing the product rule of probability, the full posterior $p(\boldsymbol{w},\boldsymbol{\gamma},\sigma^2|\boldsymbol{t})$ is written as

$$p(\boldsymbol{w},\boldsymbol{\gamma},\sigma^2|\boldsymbol{t})=p(\boldsymbol{w}|\boldsymbol{t},\boldsymbol{\gamma},\sigma^2)p(\boldsymbol{\gamma},\sigma^2|\boldsymbol{t}). \tag{6}$$

Because of computational intractability, the second term of the right-hand side in (6), for example, $p(\boldsymbol{\gamma},\sigma^2|\boldsymbol{t})$, is approximated by a Dirac delta (δ) function at its mode $\delta(\boldsymbol{\gamma}_{MP},\sigma^2_{MP})$. The values of $\boldsymbol{\gamma}_{MP}$ and σ^2_{MP} maximize

$$p(\boldsymbol{\gamma},\sigma^2|\boldsymbol{t})=\frac{p(\boldsymbol{t}|\boldsymbol{\gamma},\sigma^2)p(\boldsymbol{\gamma})p(\sigma^2)}{p(\boldsymbol{t})}. \tag{7}$$

Since $p(\boldsymbol{t})$ is independent of $\boldsymbol{\gamma}$ and σ^2, and uninformative hyperpriors over logarithms of $\boldsymbol{\gamma}$ and σ^2 are assumed, maximizing $p(\boldsymbol{\gamma}, \sigma^2|\boldsymbol{t})$ is equivalent to maximizing $p(\boldsymbol{t}|\boldsymbol{\gamma}, \sigma^2)$. The marginal likelihood $p(\boldsymbol{t}|\boldsymbol{\gamma}, \sigma^2)$ is attained by integrating $\boldsymbol{w}$ out as follows:

$$\begin{aligned} p(\boldsymbol{t}|\boldsymbol{\gamma}, \sigma^2) &= \int p(\boldsymbol{t}|\boldsymbol{w}, \sigma^2) p(\boldsymbol{w}|\boldsymbol{\gamma}) d\boldsymbol{w} \\ &= (2\pi)^{-N_s/2} \left|\sigma^2 \boldsymbol{I} + \boldsymbol{\Phi} \boldsymbol{B}^{-1} \boldsymbol{\Phi}^T\right|^{-1/2} \\ &\quad \times \exp\left(-\frac{1}{2} \boldsymbol{t}^T \left(\sigma^2 \boldsymbol{I} + \boldsymbol{\Phi} \boldsymbol{B}^{-1} \boldsymbol{\Phi}^T\right)^{-1} \boldsymbol{t}\right) \end{aligned} \tag{8}$$

where $\boldsymbol{I}$ is identity matrix. According to optimality condition, an iterative mechanism of $\boldsymbol{\gamma}$ and σ^2 is established in the following [49]:

$$\begin{cases} \gamma_{i,k+1} = \frac{\beta_{i,k}}{\mu_{i,k}^2} \\ \sigma_{k+1}^2 = \frac{\|\boldsymbol{t} - \boldsymbol{\Phi} \boldsymbol{\mu}_k\|^2}{N_s - \sum_{i=1}^{M} \beta_{i,k}} \\ \beta_{i,k} = 1 - \gamma_{i,k} \boldsymbol{\Sigma}_{ii,k} \end{cases} \tag{9}$$

where k is the step index during iteration, and $\beta_i \in [0, 1]$ is well-determinedness of parameter w_i. When a model parameter is totally influenced by the likelihood (prior), the associated β value is equal to one (zero). The iteration convergence produces $\boldsymbol{\gamma}_{MP}$ and σ_{MP}^2. Maximization of the marginal likelihood is a distinguishing facet of SBPM, which has been demonstrated to yield in most circumstances better generalization outcomes than methods using additional multifold cross-validation procedures [50].

5) Approximate Prediction Distribution: After obtaining $\boldsymbol{\gamma}_{MP}$ and σ_{MP}^2, the predictive distribution of the model output t_p is approximated by

$$\begin{aligned} p(t_p|\boldsymbol{t}) &= \int p(t_p|\boldsymbol{w}, \sigma^2) p(\boldsymbol{w}|\boldsymbol{t}, \boldsymbol{\gamma}, \sigma^2) p(\boldsymbol{\gamma}, \sigma^2|\boldsymbol{t}) d\boldsymbol{w} d\boldsymbol{\gamma} d\sigma^2 \\ &\approx \int p(t_p|\boldsymbol{w}, \sigma^2) p(\boldsymbol{w}|\boldsymbol{t}, \boldsymbol{\gamma}, \sigma^2) \delta(\boldsymbol{\gamma}_{MP}, \sigma_{MP}^2) d\boldsymbol{w} d\boldsymbol{\gamma} d\sigma^2 \\ &= \int p(t_p|\boldsymbol{w}, \sigma_{MP}^2) p(\boldsymbol{w}|\boldsymbol{t}, \boldsymbol{\gamma}_{MP}, \sigma_{MP}^2) d\boldsymbol{w} = N(\mu_p, \sigma_p^2) \end{aligned} \tag{10}$$

with

$$\begin{cases} \mu_p = \hat{y}(\boldsymbol{x}_p, \boldsymbol{\mu}) \\ \sigma_p^2 = \sigma_{MP}^2 + \boldsymbol{h}^T \boldsymbol{\Sigma} \boldsymbol{h} \end{cases} \tag{11}$$

where $\boldsymbol{x}_p$ is the model input associated with t_p, and $\boldsymbol{h} = [\varphi_1(\boldsymbol{x}_p), \ldots, \varphi_M(\boldsymbol{x}_p)]^T$. Note that $\boldsymbol{\Sigma}$ and $\boldsymbol{\mu}$ in (11) are calculated by (5), given $\boldsymbol{\gamma}_{MP}$ and σ_{MP}^2. A flowchart summarizing the aforementioned SBPM procedure is shown in Fig. 5. More theoretic and algorithmic properties of SBPM are elaborated in [50].

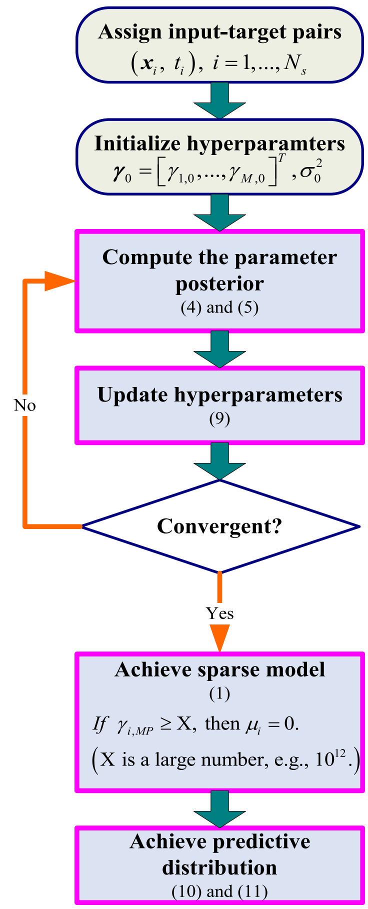

Fig. 5. SBPM flowchart.

IV. Results and Discussion

A. Bayesian SOH Estimation Model

The model target t_i is herein cell capacity, and the input $\boldsymbol{x}_i$ is voltage-sequence sample entropy (or comprises both sample entropy and cell temperature in a multivariate form). A schematic of the model training process is shown in Fig. 6. First of all, the sample entropy values of the reference cells under the HPPC excitation are calculated with respect to various aging levels. The parameters of $m = 2$, $r = 0.1$, and $N_c = 600$ are specified in the sample entropy algorithm. Note that these sample entropy values are arguably assumed to be independent of each other, as in machine learning, we often assume input features to be deterministic and independent of each other [50]. After obtaining the input–target pairs from the reference cells, the SBPM approach is exploited to learn the underlying mapping mechanism, giving rise to the SOH estimation model.

Notice that the relationship between the capacity loss and sample entropy is statically nonlinear. The key focus of machine learning, such as SBPM, is on reconstruction of the static nonlinear function between features and targets without involving dynamics [50]. The basis functions utilized in the SBPM consist of radial basis functions (RBFs) and a constant term depicted by

$$\varphi_j(\boldsymbol{x}) = \begin{cases} \exp\left(\frac{-(\boldsymbol{x} - \boldsymbol{x}_j)^2}{R^2}\right), \ j = 1, \ldots, M-1 \\ 1, \ j = M \end{cases} \tag{12}$$

where $M = N_s + 1$ and R is the RBF width. At each temperature, $N_s = 36$. The established model enables forecasting capacities of the validation cells, whereby its usefulness can be evaluated.

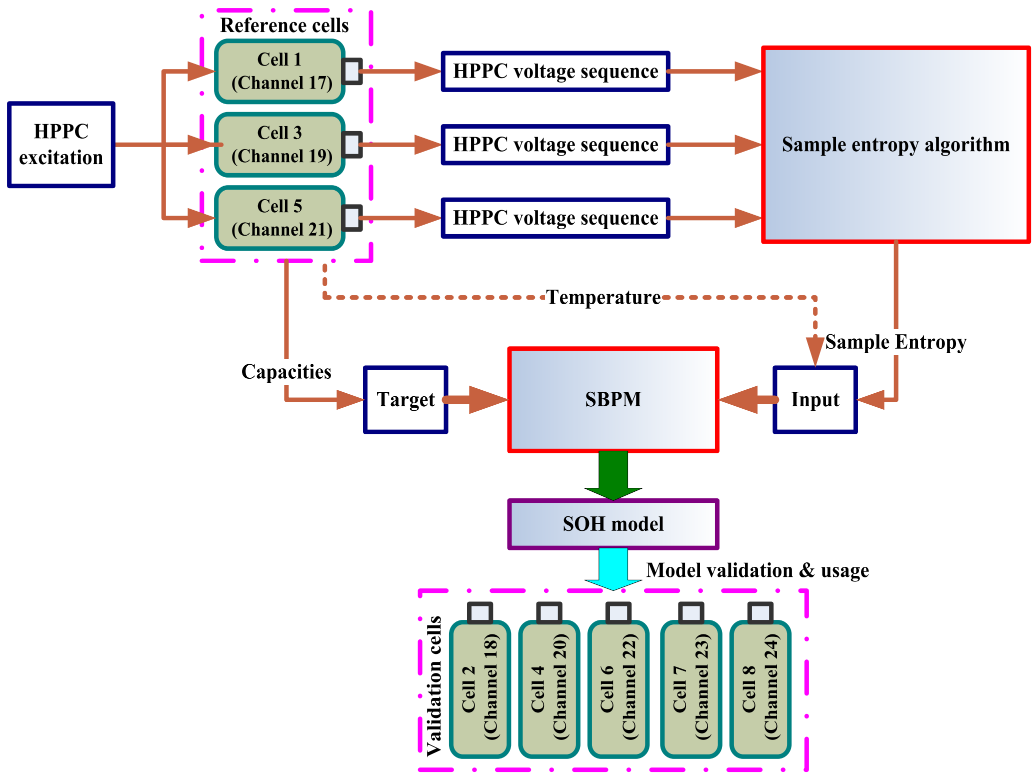

Fig. 6. Schematic of establishing the battery SOH estimation model.

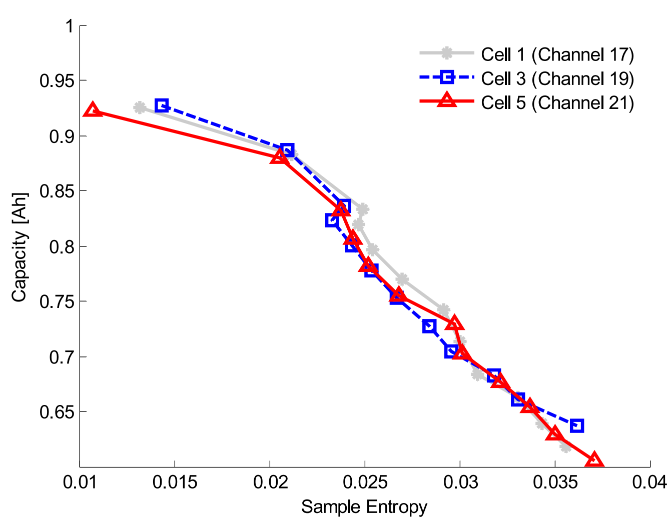

Fig. 7. Training data of the battery SOH estimation model at 10 °C.

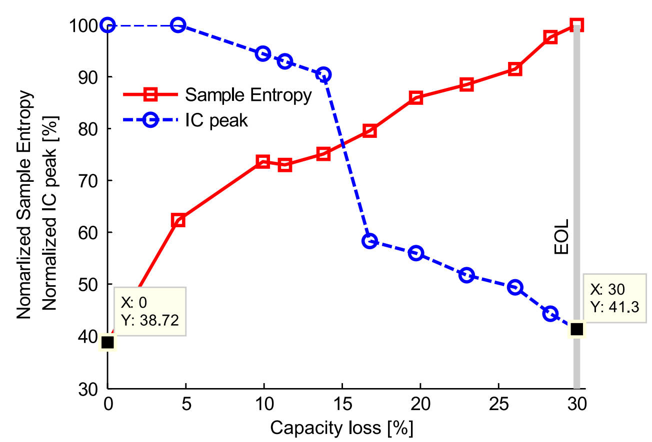

Fig. 8. Comparison of the normalized sample entropy and IC peak of cell 1 (Channel 17) at 10 °C.

The sample entropy–capacity pairs used for training the SOH model at 10 °C, for example, are given in Fig. 7. Overall, as the capacity diminishes, the sample entropy increases. Furthermore, Fig. 8 shows a comparison of the normalized sample entropy and incremental-capacity (IC) peak of cell 1 (Channel 17) at 10 °C (the latter has been demonstrated to be an effectual signature indicative of battery capacity loss in [37] and [40]). The sample entropy exhibits a comparable (even slightly higher) sensitivity to capacity loss and is thus as arguably informative as IC peak. Similar results are found at other temperatures and for other cells. A closer examination discloses that the correlation between the sample entropy and capacity is nonlinear, leading to a nontrivial modeling task where the SBPM approach comes to the forth. The outcome of maximizing the marginal likelihood $p(\boldsymbol{t}|\gamma, \sigma^2)$ is illustrated in Fig. 9, together with the optimized data noise σ^2_{MP}. The relevant parameters identified and levels of well-determinedness are shown in Fig. 10. It is noticeable that the SBPM approach contributes to a sparse model with just four relevant parameters, and their uncertainties are quantified. The modeling outcome in the training data is indicated in Fig. 11. It can be seen that the model is a concise (smooth) but accurate way to correlate the sample entropy to the cell capacity in the training data. As similar training results are observed at 22 °C and 35 °C, they are omitted for simplicity.

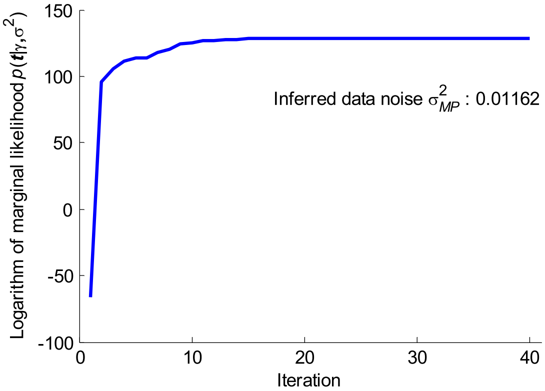

Fig. 9. Maximization of the marginal likelihood $p(\boldsymbol{t}|\gamma, \sigma^2)$ at 10 °C.

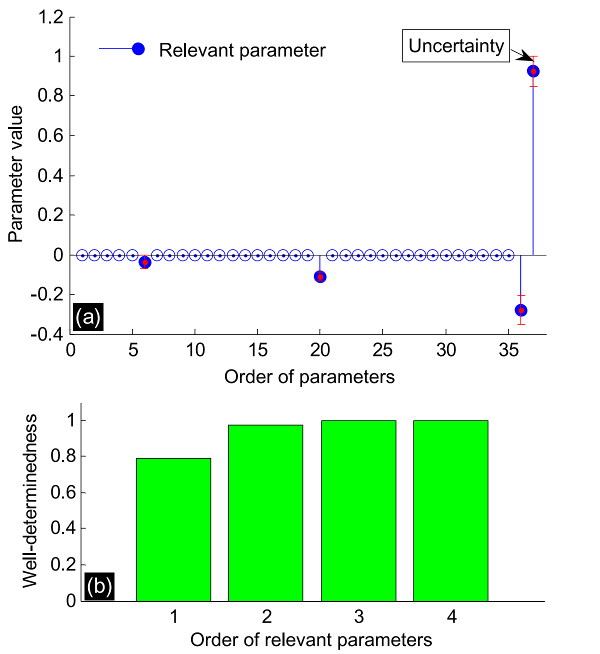

Fig. 10. (a) Model parameters, and (b) well-determinedness at 10 °C.

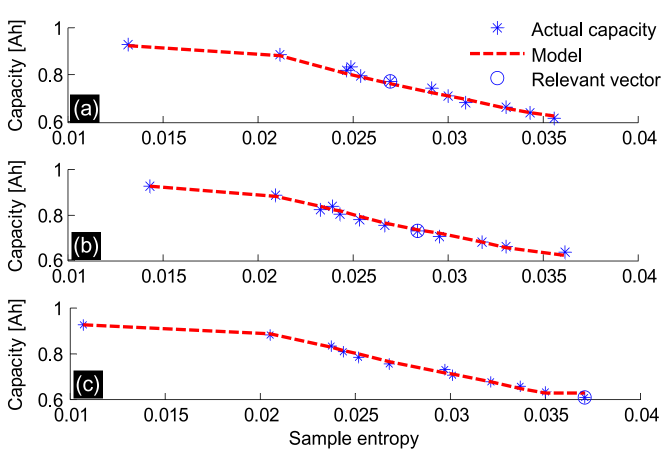

Fig. 11. Modeling outcome in the training data at 10 °C: (a) cell 1, (b) cell 3, and (c) cell 5. Relevant vector denotes the training data point corresponding to a nonzero (relevant) model parameter.

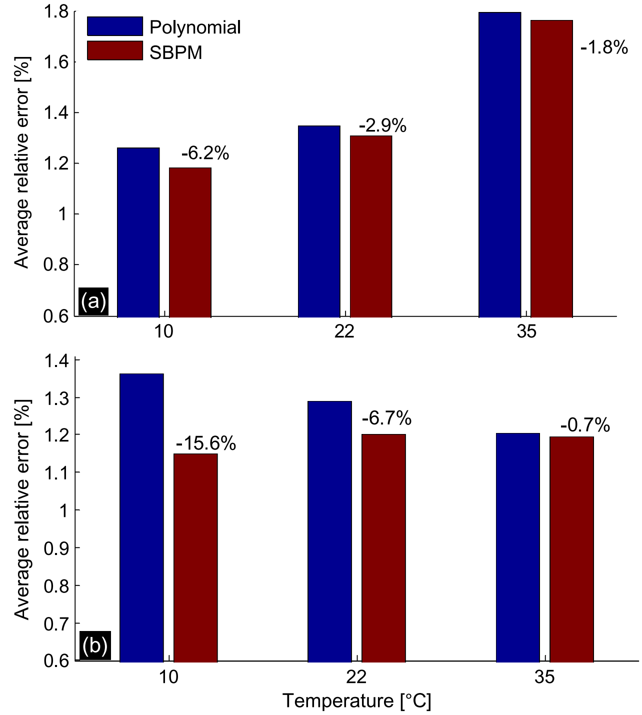

Fig. 12. Comparison between the SBPM and third-order polynomial model: (a) Training outcome (cells 1, 3, and 5), and (b) validation outcome (cells 2, 4, 6, 7, and 8).

In our prior work [43], a third-degree polynomial SOH model was carefully developed, which has proven to be a preferable choice in the family of polynomials. The comparison results between the two models in both training and validation data are presented in Fig. 12. In contrast to the polynomial model, the average relative capacity errors in the SBPM approach decrease approximately 6.2%, 2.9%, and 1.8% at 10 °C, 22 °C, and 35 °C in the training data, respectively. More significantly, the improvements in validation are about 15.6%, 6.7%, and 0.7%. Both models have almost the same complexity. These facts signify that the SBPM is able to better excavate the useful information in the training data without unnecessary complexity, therefore delivering improved extrapolation and generalization.

B. Analytical Integration of Temperature Effects

Another advantage of the SBPM over polynomial models is the great flexibility of expanding the model input variables. For instance, temperature effects can be readily incorporated into the SBPM framework in a closed form, i.e., $\boldsymbol{x}_i$ includes both the sample entropy and cell temperature. As a consequence, instead of separately creating one model at each temperature, a unified SBPM-based SOH model that is explicitly temperature-aware can be established. In this scenario, the training data encompass all the input–target pairs of the reference cells at the three temperatures. The maximization of the marginal likelihood $p(\boldsymbol{t}|\gamma, \sigma^2)$ and estimated data noise variance are presented in Fig. 13. The relevant model parameters are given in Fig. 14. Albeit much more training data, the model sparsity is still obvious. As conveyed in Fig. 15, the model provides very precise capacity estimates for all the cells at the three temperatures.

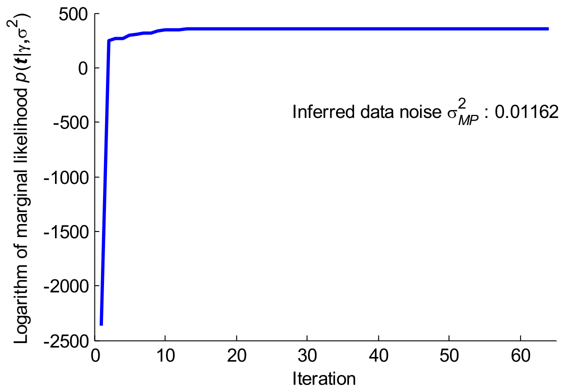

Fig. 13. Maximization of the marginal likelihood $p(\boldsymbol{t}|\gamma, \sigma^2)$ at all the three temperatures.

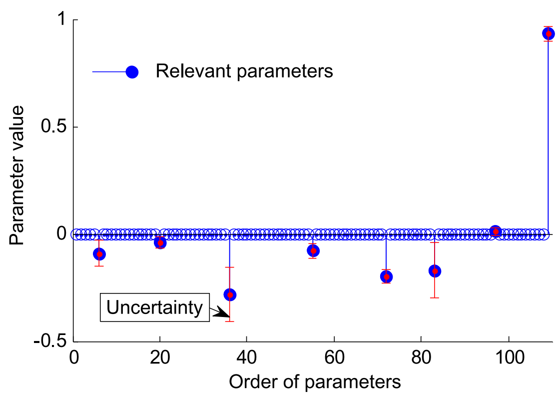

Fig. 14. Parameters of the temperature-aware SPBM.

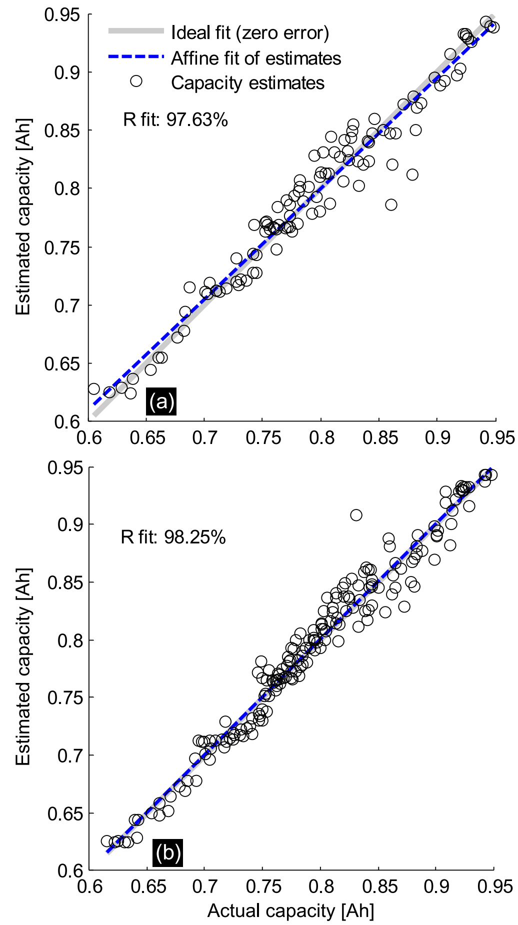

Fig. 15. Training and validation results at all the three temperatures: (a) Training (cells 1, 3, and 5), and (b) validation (cells 2, 4, 6, 7, and 8).

To further verify the effectiveness of the temperature-aware SBPM, a comparison with the SVM counterpart is conducted. As a state-of-the-art kernel technique for nonlinear mapping, the SVM model is considered for benchmarking purposes. Note that both models adopt the identical RBF functions and training/validation data. The hyperparameters in the SVM model (namely, insensitive zone and regularization factor) are determined by tenfold cross validation. The SVM model is implemented by LIBSVM [51].

The comparison result is listed in Table III. Apparently, the SBPM model ensures comparable (even slightly better) performance with considerably less complexity. As opposed to the SVM model, the SBPM showcases additional benefits, such as notably a probabilistic modeling scenario enabling uncertainty quantification, avoiding time-consuming and heuristic cross validation for fixing hyperparameters, and no requirement for only using Mercel kernel functions.

TABLE III
COMPARISON BETWEEN SBPM AND SVM

		SBPM	SVM
Average relative capacity error [%]	Training	1.61	1.66
	Validation	1.38	1.48
Number of relevant parameters	-	8	25

C. RUL Prediction

The RUL is defined as the remaining life until the cell arrives at its End-of-Life (EOL). In this paper, 30% capacity (SOH) loss is chosen as the EOL criterion. Given a trajectory of SOH estimates $\{\hat{h}_j|j = 1, \ldots, N_h\}$ provided by the SBPM, the RUL can be deduced by projecting the SOH estimates out into the future until the EOL (70% SOH) is reached. Thus, the idea is to apply an affine regression to fit the trajectory of SOH estimates $\{\hat{h}_j|j = 1, \ldots, N_h\}$ as follows:

$$\hat{h}(C_l) = q_0 + q_1 C_l \tag{13}$$

where C_l is the cycle number, and q_0 and q_1 are two unknown coefficients to be calibrated. After obtaining the two coefficients, the RUL can be estimated by subtracting the number already cycled from the solution of $\hat{h}(C_l) = 70\%$. Because the RUL is intrinsically stochastic, a bootstrap sampling technique is adopted to randomly generate multiple trajectories of SOH $\{\hat{h}^*_j|j = 1, \ldots, N_h\}$ via sampling the trajectory $\{\hat{h}_j|j = 1, \ldots, N_h\}$ with replacement. Here, 100 of such trajectories are generated at each forecasting point. Accordingly, 100 RUL predictors are constructed to derive the probabilistic characteristics of RUL. As an example, the RUL prediction result of cell 2 (Channel 18, one of validation cells) at 10 °C is illustrated in Fig. 16. When the prediction starts at 452 cycles,

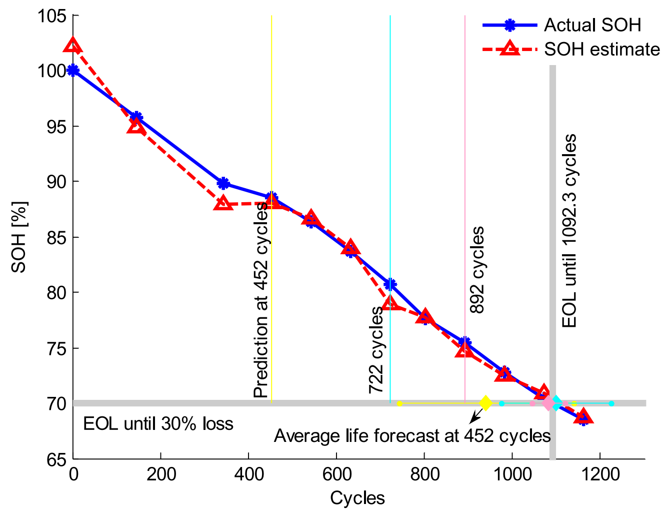

Fig. 16. RUL prediction result of cell 2 (Channel 18, one of validation cells) at 10 °C.

the RUL has relatively large standard deviation, and its average is underestimated, because the SOH estimate has a more steep decrease than the actual SOH until 452 cycles. However, as more SOH estimates become available, the predicted RUL has a shrinking standard deviation, and its average has excellent agreement with the true one (e.g., see the predictions at 722 and 892 cycles).

V. Conclusion

A synergy of sample entropy and SBPM has been exploited to synthesize a data-driven battery SOH estimator. Large amounts of testing data at three different temperatures from multiple cells have been used to verify its performance. The result shows that the estimator is accurate and robust (the average error is less than 1.2% at each temperature). It also has been corroborated that the SBPM-based estimator outperforms the third-degree polynomial model in both training and validation processes. The proposed approach enables an explicitly temperature-aware SOH estimator by an analytical integration of temperature effects. Compared with the SVM scheme, such a multivariate SBPM estimator exhibits comparable (even slightly better) performance with much simpler and sparser topology. Additional advantages include a probabilistic model representation, removal of heuristically time-consuming tuning, and flexibility of choosing kernel functions. In conjunction with bootstrap sampling, the developed SOH estimator makes it possible to predict the battery RUL in a probabilistic manner. The predicted RUL is satisfactory in terms of its average and spread.

The future work could be the consideration of more temperature points to further examine the temperature dependence of the multivariate SOH predictor.

Acknowledgment

The authors would like to thank Prof. H. Peng at the University of Michigan, Ann Arbor, MI, USA, for kindly sharing the battery testing facility and data.

References

[1] S. M. Lukic, J. Cao, R. C. Bansal, F. Rodriguez, and A. Emadi, “Energy storage systems for automotive applications,” *IEEE Trans. Ind. Electron.*, vol. 55, no. 6, pp. 2258–2267, Jun. 2008.

[2] S. Vazquez, S. M. Lukic, E. Galvan, L. G. Franquelo, and J. M. Carrasco, “Energy storage systems for transport and grid applications,” *IEEE Trans. Ind. Electron.*, vol. 57, no. 12, pp. 3881–3895, Dec. 2010.

[3] X. Lu, K. Sun, J. M. Guerrero, J. C. Vasquez, and L. Huang, “State-of-charge balance using adaptive droop control for distributed energy storage systems in DC microgrid applications,” *IEEE Trans. Ind. Electron.*, vol. 61, no. 6, pp. 2804–2815, Jun. 2014.

[4] X. Hu, L. Johannesson, N. Murgovski, and B. Egardt, “Longevity-conscious dimensioning and power management of the hybrid energy storage system in a fuel cell hybrid electric bus,” *Appl. Energy*, vol. 137, pp. 913–924, Jan. 2015.

[5] H. Rahimi-Eichi, U. Ojha, F. Baronti, and M. Chow, “Battery management system: An overview of its application in the smart grid and electric vehicles,” *IEEE Ind. Electron. Mag.*, vol. 7, no. 2, pp. 4–16, Jun. 2013.

[6] S. Haghbin, S. Lundmark, M. Alaküla, and O. Carlson, “Grid-connected integrated battery chargers in vehicle applications: Review and new solution,” *IEEE Trans. Ind. Electron.*, vol. 60, no. 2, pp. 459–473, Feb. 2013.

[7] X. Hu, F. Sun, and X. Cheng, “Recursive calibration for a lithium iron phosphate battery for electric vehicles using extended Kalman filtering,” *J. Zhejiang Univ. Sci. A*, vol. 12, no. 11, pp. 818–825, 2011.

[8] S. J. Moura and H. Z. Perez, “Better battery through electrochemistry,” *ASME Dyn. Syst. Control Mag.*, vol. 2, no. 2, pp. 15–21, 2014.

[9] F. Zhang, G. Liu, L. Fang, and H. Wang, “Estimation of battery state of charge with H_∞ observer: Applied to a robot for inspecting power transmission lines,” *IEEE Trans. Ind. Electron.*, vol. 59, no. 2, pp. 1086–1095, Feb. 2012.

[10] M. Gholizadeh and F. R. Salmasi, “Estimation of state of charge, unknown nonlinearities, and state of health of a lithium-ion battery based on a comprehensive unobservable model,” *IEEE Trans. Ind. Electron.*, vol. 61, no. 3, pp. 1335–1344, Mar. 2014.

[11] H. Rahimi-Eichi, F. Baronti, and M. Chow, “Online adaptive parameter identification and state-of-charge coestimation for lithium-polymer battery cells,” *IEEE Trans. Ind. Electron.*, vol. 61, no. 4, pp. 2053–2061, Apr. 2014.

[12] X. Hu and F. Sun, “Fuzzy clustering based multi-model support vector regression state of charge estimator for lithium-ion battery of electric vehicle,” in *Proc. IEEE Int. Conf. Intell. Human-Mach. Syst. Cybern.*, Hangzhou, China, Aug. 26–27, 2009, pp. 392–396.

[13] X. Hu, R. Xiong, and B. Egardt, “Model-based dynamic power assessment of lithium-ion batteries considering different operating conditions,” *IEEE Trans. Ind. Informat.*, vol. 10, no. 3, pp. 1948–1959, Aug. 2014.

[14] S. Li, B. Wang, H. Peng, and X. Hu, “An electrochemistry based impedance model for lithium ion batteries,” *J. Power Sources*, vol. 258, pp. 9–18, Jul. 2014.

[15] S. Yin, H. Luo, and S. X. Ding, “Real-time implementation of fault-tolerant control systems with performance optimization,” *IEEE Trans. Ind. Electron.*, vol. 61, no. 5, pp. 2402–2411, May 2014.

[16] S. Yin, S. X. Ding, X. Xie, and H. Luo, “A review on basic data-driven approaches for industrial process monitoring,” *IEEE Trans. Ind. Electron.*, vol. 61, no. 11, pp. 6418–6428, Nov. 2014.

[17] S. Yin, X. Li, H. Gao, and O. Kaynak, “Data-based techniques focused on modern industry: An overview,” *IEEE Trans. Ind. Electron.*, vol. 62, no. 1, pp. 657–667, Jan. 2015.

[18] Y. Wang, G. Ma, S. X. Ding, and C. Li, “Subspace aided data-driven design of robust fault detection and isolation systems,” *Automatica*, vol. 47, no. 11, pp. 2474–2480, Nov. 2011.

[19] Y. Wang, B. Gao, and H. Chen, “Data-driven design of parity space-based FDI system for AMT vehicles,” *IEEE/ASME Trans. Mechatronics*, vol. 20, no. 1, pp. 405–415, Feb. 2015.

[20] A. Barré *et al.*, “A review on lithium-ion battery ageing mechanisms and estimations for automotive applications,” *J. Power Sources*, vol. 241, pp. 680–689, Nov. 2013.

[21] S. M. Rezvanizaniani, Z. Liu, Y. Chen, and J. Lee, “Review and recent advances in battery health monitoring and prognostics technologies for electric vehicle (EV) safety and mobility,” *J. Power Sources*, vol. 256, pp. 110–124, Jun. 2014.

[22] K. S. Ng, C. S. Moo, Y. P. Chen, and Y. C. Hsieh, “Enhanced coulomb counting method for estimating state-of-charge and state-of-health of lithium-ion batteries,” *Appl. Energy*, vol. 86, no. 9, pp. 1506–1511, Sep. 2009.

[23] J. Christensen and J. Newman, "Effect of anode film resistance on the charge/discharge capacity of a lithium-ion battery," *J. Electrochem. Soc.*, vol. 150, no. 11, pp. A1416–A1420, 2003.

[24] J. Christensen and J. Newman, "A mathematical model for the lithium-ion negative electrode solid electrolyte interphase," *J. Electrochem. Soc.*, vol. 151, no. 11, pp. A1977–A1988, 2004.

[25] M. Safari and C. Delacourt, "Simulation-based analysis of aging phenomena in a commercial graphite/LiFePO4 cell," *J. Electrochem. Soc.*, vol. 158, no. 12, pp. A1436–A1447, 2011.

[26] J. Wang *et al.*, "Cycle-life model for graphite-LiFePO4 cells," *J. Power Sources*, vol. 196, no. 8, pp. 3942–3948, Apr. 2011.

[27] M. Safari, M. Morcrette, A. Teyssot, and C. Delacourt, "Life-prediction methods for lithium-ion batteries derived from a fatigue approach I. Introduction: Capacity-loss prediction based on damage accumulation," *J. Electrochem. Soc.*, vol. 157, no. 6, pp. A713–A720, 2010.

[28] G. L. Plett, "Extended Kalman filtering for battery management systems of LiPB-based HEV battery packs: Part 3. State and parameter estimation," *J. Power Sources*, vol. 134, no. 2, pp. 277–292, Aug. 2004.

[29] I. S. Kim, "A technique for estimating the state of health of lithium batteries through a dual-sliding-mode observer," *IEEE Trans. Power Electron.*, vol. 25, no. 4, pp. 1013–1022, Apr. 2010.

[30] B. Saha and K. Goebel, "Modeling Li-ion battery capacity depletion in a particle filtering framework," in *Proc. Annu. Conf. Prognostics Health Manage. Soc.*, San Diego, CA, USA, Sep. 27–Oct. 1, 2009, pp. 1–10.

[31] M. Rezvani, M. AbuAli, S. Lee, J. Lee, and J. Ni, "A comparative analysis of techniques for electric vehicle battery prognostics and health management (PHM)," Soc. Automotive Eng. (SAE) Int., Warrendale, PA, USA, Tech. Paper 2011-01-2247, 2011.

[32] W. He, N. Williard, M. Osterman, and M. Pecht, "Prognostics of lithium-ion batteries based on Dempster-Shafer theory and the Bayesian Monte Carlo method," *J. Power Sources*, vol. 196, no. 23, pp. 10 314–10 321, Dec. 2011.

[33] D. Andre, A. Nuhic, T. Soczka-Guth, and D. U. Sauer, "Comparative study of a structured neural network and an extended Kalman filter for state of health determination of lithium-ion batteries in hybrid electric vehicles," *Eng. Appl. Artif. Intell.*, vol. 26, no. 3, pp. 951–961, Mar. 2013.

[34] H. T. Lin, T. J. Liang, and S. M. Chen, "Estimation of battery state of health using probabilistic neural network," *IEEE Trans. Ind. Inf.*, vol. 9, no. 2, pp. 679–685, May 2013.

[35] A. J. Salkind, C. Fennie, P. Singh, T. Atwater, and D. E. Reisner, "Determination of state-of-charge and state-of-health of batteries by fuzzy logic methodology," *J. Power Sources*, vol. 80, no. 1/2, pp. 293–300, Jul. 1999.

[36] A. Nuhic, T. Terzimehic, T. Soczka-Guth, M. Buchholz, and K. Dietmayer, "Health diagnosis and remaining useful life prognostics of lithium-ion batteries using data-driven methods," *J. Power Sources*, vol. 239, pp. 680–688, Oct. 2013.

[37] E. M. Krieger, J. Cannarella, and C. B. Arnold, "A comparison of lead-acid and lithium-based battery behavior and capacity fade in off-grid renewable charging applications," *Energy*, vol. 60, pp. 492–500, Oct. 2013.

[38] I. Bloom *et al.*, "Differential voltage analyses of high-power, lithium-ion cells: 1. Techniques and application," *J. Power Sources*, vol. 139, no. 1/2, pp. 295–303, Jan. 2005.

[39] B. Wu *et al.*, "Differential thermal voltammetry for tracking of degradation in lithium-ion batteries," *J. Power Sources*, vol. 273, pp. 495–501, Jan. 2015.

[40] C. Weng, Y. Cui, J. Sun, and H. Peng, "On-board state of health monitoring of lithium-ion batteries using incremental capacity analysis wit support vector regression," *J. Power Sources*, vol. 235, pp. 36–44, Aug. 2013.

[41] A. Barré, F. Suard, M. Gérard, M. Montaru, and D. Riu, "Statistical analysis for understanding and predicting battery degradations in real-life electric vehicle use," *J. Power Sources*, vol. 245, pp. 846–856, Jan. 2014.

[42] A. Widodo, M. C. Shim, W. Caesarendra, and B. S. Yang, "Intelligent prognostics for battery health monitoring based on sample entropy," *Expert Syst. Appl.*, vol. 38, no. 9, pp. 11 763–11 769, Sep. 2011.

[43] X. Hu, S. Li, Z. Jia, and B. Egardt, "Enhanced sample entropy-based health management of Li-ion battery for electrified vehicles," *Energy*, vol. 64, pp. 953–960, Jan. 2014.

[44] X. Xie, S. Yin, H. Gao, and O. Kaynak, "Asymptotic stability and stabilisation of uncertain delta operator systems with time-varying delays," *IET Control Theory A*, vol. 7, no. 8, pp. 1071–1078, May 2013.

[45] X. Hu, S. Li, and H. Peng, "A comparative study of equivalent circuit models for Li-ion batteries," *J. Power Sources*, vol. 198, pp. 359–367, Jan. 2012.

[46] F. Baronti, G. Fantechi, R. Roncella, and R. Saletti, "High-efficiency digitally controlled charge equalizer for series-connected cells based on switching converter and super-capacitor," *IEEE Trans. Ind. Informat.*, vol. 9, no. 2, pp. 1139–1147, May 2013.

[47] F. Baronti *et al.*, "Design and safety verification of a distributed charge equalizer for modular Li-ion batteries," *IEEE Trans. Ind. Informat.*, vol. 10, no. 2, pp. 1003–1011, May 2014.

[48] J. S. Richman and J. R. Moorman, "Physiological time series analysis using approximate entropy and sample entropy," *Amer. J. Physiol.*, vol. 278, no. 6, pp. H2039–H2049, Jun. 2000.

[49] M. E. Tipping and A. C. Faul, "Fast marginal likelihood maximisation for sparse Bayesian models," in *Proc. 9th Int. Workshop Artif. Intell. Statist.*, Key West, FL, USA, Jan. 2003, pp. 1–13.

[50] M. E. Tipping, "Sparse Bayesian learning and the relevance vector machine," *J. Mach. Learn. Res.*, vol. 1, pp. 211–244, Jun. 2001.

[51] C. C. Chang and C. J. Lin, "LIBSVM: A library for support vector machines," *ACM Trans. Intell. Syst. Technol.*, vol. 2, no. 3, pp.1–27, Apr. 2011.

Xiaosong Hu (S'11–M'13) received the Ph.D. degree in automotive engineering from Beijing Institute of Technology, Beijing, China, in 2012.

He conducted scientific research and completed his Ph.D. dissertation in the Automotive Research Center at the University of Michigan, Ann Arbor, MI, USA, between 2010 and 2012. He is currently a Postdoctoral Scholar with the Department of Civil and Environmental Engineering, University of California, Berkeley, CA, USA. He was a Postdoctoral Researcher with the Swedish Hybrid Vehicle Center and the Department of Signals and Systems at Chalmers University of Technology, Gothenburg, Sweden, between 2012 and 2014. He was also a Visiting Postdoctoral Researcher with the Institute for Dynamic Systems and Control, Swiss Federal Institute of Technology (ETH), Zurich, Switzerland, in 2014. His research interests include modeling and control of alternative-energy powertrains and energy storage systems.

Dr. Hu was the recipient of the Beijing Best Ph.D. Dissertation Award in 2013.

Jiuchun Jiang (M'10–SM'14) was born in Jilin Province, China. He received the B.S. degree in electrical engineering and the Ph.D. degree in power system automation from Northern Jiaotong University, Beijing, China, in 1993 and 1999, respectively.

He is currently a Professor with the School of Electrical Engineering, Beijing Jiaong University, Beijing. His main interests are related to battery application technology, electric car charging stations, and microgrid technology.

Dr. Jiang was the recipient of the National Science and Technology Progress Second Award for his work on an EV bus system, and the Beijing Science and Technology Progress Second Award for his work on an EV charging system.

Dongpu Cao (M'08) received the Ph.D. degree from Concordia University, Montreal, QC, Canada, in 2008.

He was a Canada NSERC and Ontario MRI Fellow with the University of Waterloo, Waterloo, ON, Canada, between 2008 and 2011. From May 2011 to February 2014, he was a Lecturer and Director of Studies in the M.Sc. Mechanical Engineering Program with Lancaster University, Lancaster, U.K. Since March 2014, he has been a Lecturer in alternative powertrain and energy optimization at the Centre for Automotive Engineering, Cranfield University, Bedford, U.K. His research focuses mainly on electric/hybrid vehicles, vehicle dynamics/control, and intelligent vehicles.

Dr. Cao was the recipient of the ASME AVTT2010 Best Paper Award and 2012 SAE Arch T. Colwell Merit Award. He serves as an Editor for the IEEE TRANSACTIONS ON VEHICULAR TECHNOLOGY, an Associate Editor for the IEEE TRANSACTIONS ON INDUSTRIAL ELECTRONICS and *International Journal of Vehicle Design*, and an Editorial Board member for four other journals. He was a Guest Editor for Vehicle System Dynamics between 2008 and 2010, and is a Guest Editor for the IEEE/ASME TRANSACTIONS ON MECHATRONICS.

Bo Egardt (SM'90–F'03) received the M.Sc. degree in electrical engineering and the Ph.D. degree in automatic control from Lund Institute of Technology, Lund, Sweden, in 1974 and 1979, respectively.

During 1980, he was a Research Associate with the Information Systems Laboratory, Stanford, CA, USA. From 1981 to 1989, he was with Asea Brown Boveri (ABB), where he was heavily involved in the introduction of adaptive control in the process industry. Since 1989, he has been a Professor and the Head of the Automatic Control Group, Chalmers University of Technology, Gothenburg, Sweden. He is also the Head of the Group of Systems and Control in the Swedish Hybrid Vehicle Center. His main areas of interest include system identification, adaptive and optimal control, and applications of control in the automotive field.

Dr. Egardt has been an Associate Editor of the IEEE TRANSACTIONS ON CONTROL SYSTEMS TECHNOLOGY and of the *European Journal of Control*. He is a member of the Editorial Board of the *International Journal of Adaptive Control and Signal Processing*. He is an Academician of the Royal Swedish Academy of Engineering Sciences.